Technical Report NCSU-ERL-95-19

A Micro-machined Approach to Optical Interconnect

David A. Winick W. Michael Teague Paul D. Franzon

Electronics Research Laboratory
http://www2.ncsu.edu/eos/project/erl
Department of Electrical and Computer Engineering
North Carolina State University
Box 7911 Raleigh, NC 27695

Abstract — This paper describes several innovative optical modulator devices for reconfigurable free-space interconnect, in an effort to demonstrate both the technology limitations and the performance advantages available via this application of microelectromechanical systems.

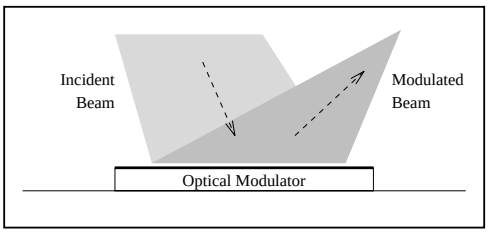

Figure 1: Reflective Free-space Optical Modulator

1 Introduction

With the increase of transistor counts and device speeds, there is an increasing need for multi-ported high-speed interconnection. And in many applications it is most desirable for the interconnection to be reconfigurable, enabling high-bandwidth channels between devices while maintaining low signal latencies.

There is also an increasing need for devices to be characteristically low-power and highly reliable. This is due to the explosion of portable computing devices appearing in the marketplace, and a resulting desire for increased versatility.

It is suggested in this paper that microelectromechanical systems (from here on, referred to as MEMS) technology can serve as a solution to providing high-speed optical interconnect in applications that require reconfigurability and low power consumption. Applications range from ATM switch networks, to laser printer scanning, to visual display generation.

In this paper we will describe several high-speed optical interconnect switches. The switches are reflective-mode free-space optical modulator structures, fabricated through a standard microelectromechanical machining process. The design criteria, application, and expected performance of these devices are briefly examined.

2 Fabrication

Surface micro-machining is a process by which a structure of thin film materials layered on a substrate is subjected to a final fabrication stage that etches away any exposed sacrificial material. This final etch of chosen material results in movable mechanical structures, as shown in example Figures 2 and 3. Mechanical actuation of these structures can be transduced from electrical energy sources (voltage or current) through several principles: by electrostatics, electromagnetics, piezoelectrics, or thermomechanics. In this paper we present elements that incorporate electrostatic mechanisms.

This process by which we created the elements discussed below consists of layers as described in Table 1. Layers in the table are listed in the order in which they appear structurally (i.e., in the reverse order by which they are deposited and etched). The polysilicon layers, deposited via LPCVD, are Phosphorus doped and annealed for reduced internal stresses and fine grain size. Reactive ion etching (RIE) is used to pattern all of the layers, except the metal and nitride. The metal is patterned by lift-off. And the nitride layer acts to isolate the structure from the substrate, and is consequently unpatternable. The process also includes the ability to etch dimples, 7500Å deep, into the first layer of oxide; the use of this etch will be discussed in the next section.

Layer Name	*Size* (Å)	*Layer Description*
Metal	5000	Gold metalization
Cr	200	Chromium adhesion
Poly2	14800	2^{nd} structural layer
Oxide2	5000	Polysilicate-glass (PSG)
Poly1	20175	1^{st} structural layer
Oxide1	20000	Polysilicate-glass (PSG)
Poly0	5450	0^{th}-layer polysilicon
Nitride	4940	Isolation layer
Wafer	—	$1cm$ x $1cm$ Si substrate

Table 1: MUMPS5 Process Layers

3 Device Designs

The elements discussed here are designed to deflect free-space coherent optical beams using one of three methods:

- rotational shift of a holographic diffractor
- angular repositioning of a reflector
- reprogramming of a holographic diffractor

Design of components with these methods and applications face many concerns. The first of which are inherent in a MEMS process:

Deposition methods: effects on edge shape, film thickness, and mechanical properties

Etching methods: resulting surface quality, and mechanical stiction

Actuation methods: drive control complexity and speed, static or dynamic vibration modes

There are also optical issues that must be confronted:

holographic coding scheme: Computer generated holographic elements (CGH's) built in MEMS must be designed to fit the application.

scanning scheme: Speed of mechanical actuation is a dominating factor, and multiplexing of elements may be necessary.

loss from mechanical support structures: Exposure of supportive structures to incident beam should be minimized or in such a way as to not interfere with function of reflective structures.

mechanical stability losses: Unless elements are to be operated in dynamic mode (vibrating), their design must incorporate states of relative stability, at points they contribute to the optical function of the modulator.

activation of semiconductor material: If an application requires modulation of a high-energy beam, energy from that beam must not be allowed to inhibit proper electronic control of elements.

optical reflectivity: Materials, layering schemes, and thicknesses must be designed to optimize optical efficiencies.

And finally, issues of yield and process deviation that go into building element arrays, as we have built here:

alignment of modulator: Fabrication must result in an accurate implementation of the intended design.

repeatability of elements: Each element in the arrays must exhibit similar control responses.

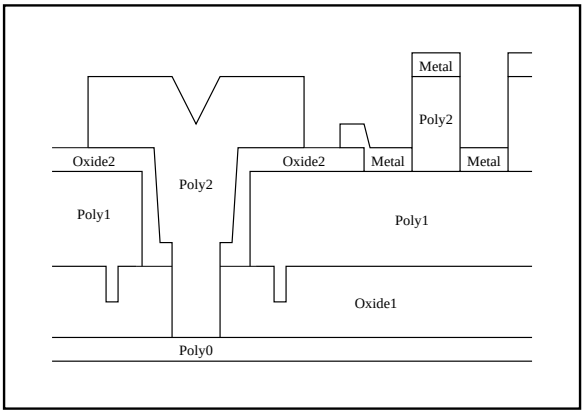

Figure 2: Axle Design before Release

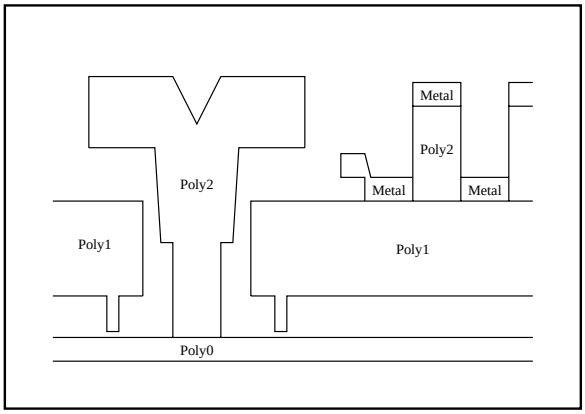

Figure 3: Axle Design after Release

3.1 Optical-alignment Grating

Let us first discuss the creation of simple grating structures in MEMS. The gratings are built of supportive polysilicon structures beneath a layer of metal, where the Au acts to reflect approximately 97% of a $632.8nm$ wavelength beam. We have attempted to use Al as the reflective metal, but found its surface to be too rough due to its lack of resistance to HF, which is required in the final release stage of fabrication to etch sacrificial oxide. An incident beam is diffracted by the grating into many orders of light, at angles according to the grating equation:

$$d\sin(\alpha) + d\sin(\beta) = m\lambda \qquad (1)$$

where d is the grating period, α the incident angle, β the reflected angle, m the order, and λ the wavelength.

Figures 2, 4, and 5 show the three possible methods in the given process for building supporting structures for a reflective metal surface that forms a repeating step function. The grating of Figure 2 can be found in its upper right-hand corner. It is desirable to form sharp edges, with little reflectivity on the vertical surfaces; and the very directional deposition method (evaporation) of the reflective metal allows such a structure. Steep vertical surface must also be built. By minimizing the number of intermediate layers between the patterned layer, defining the grating structure, and the reflecting surface material, this can be achieved. However, while the grating in Figure 2 may employ the fewest number of intermediate layers (none), it also suffers from a 150% over-etch of Poly2. The over-etch is necessary to prevent stringers and other non-uniformities in other polysilicon structures. The result, in this case, is a very deep step structure. Thus, assuming a $4\mu m$ grating period, any light beyond about 15 deg from the normal will be lost due to the depth.

If the lower portion of the step function is to serve as an additive component to the diffracted beam function, it should be at a distance from the top which is an odd multiple of approximately $\frac{\lambda}{4}$, where λ is the wavelength of the incident beam. This would reflect half of the incident wave at $\frac{1}{2}$ phase offset, resulting in a 4-fold improvement in irradiance. The etch in Figure 2 is too thick for this necessary accuracy. Shallower grating structures can be built in this process by either patterning Poly1, as in Figure 5, or Oxide2, as in Figure 4. While the latter allows for the largest diffraction efficiencies, it is only optimum, in the visible spectra, for frequencies at each end of this range (at 400nm and 667nm).

3.2 Movable Diffraction Elements

The grating design in Figure 2 also suffers from mechanical instability if it is to be placed on a mechanically mobile structure. Figure 6 shows an example of how such a structure might be layed out. In this figure, the large shaded disk is an area of Poly1 covered by a grating structure. This disk is designed to be electrostatically rotated about a central axle via voltage applied to stators. The stators form a ring about the grating perimeter. Figures 2 and 7 show designs of the axle and stator, respectively. Note that the grating structure shown in Figure 2 would result in etches that go completely through the Poly1 disk, and would be inapropriate for such an element, as explained above.

By building a grating structure on top of a disk that can rotate in the plane of the wafer, diffracted beams can be deflected in directions defined by conical arcs about the surface normal. Furthermore, modifying the design from simple grating to hologram would increase optical efficiency, and would focus most of the optical energy into a particular

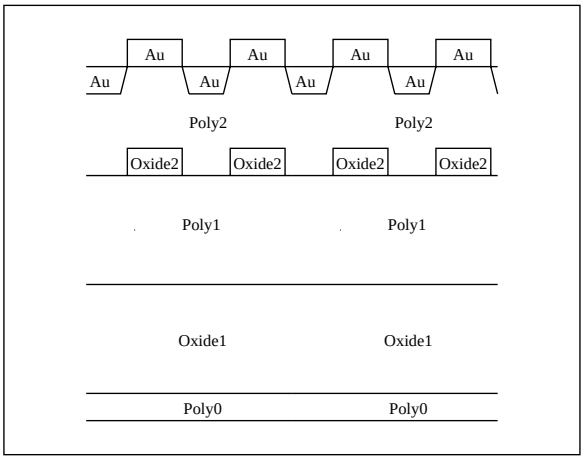

Figure 4: 0.5 micron deep Grating Design

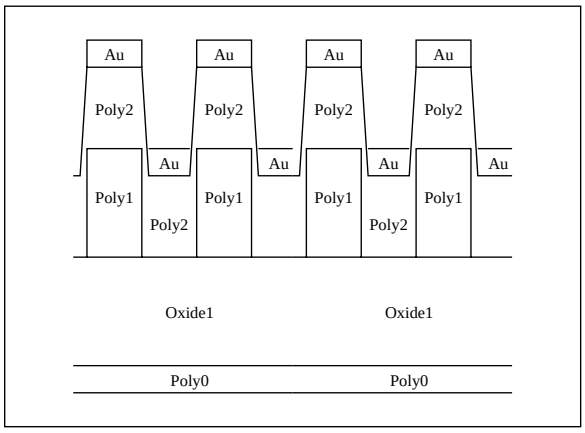

Figure 5: 2.0 micron deep Grating Design

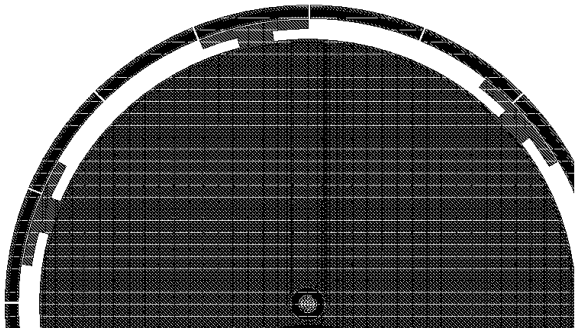

Figure 6: Portion of Rotating Grating Layout

diffracted order. A typical 1-to-n optical switch for this arrangement would require n photodiodes to be arranged about this cone.

The only resistance to actuation of this device is friction. Friction, and stiction (resistance to first-time actuation), of the disk to Poly0, below, is reduced by dimpling Oxide1 in key areas before subsequent processing; this results in pegs of Poly1 on which the rest of the disk stands. The pegs reduce contact area and thus friction.

Application of opposite charges to opposing stators would cause the rotor to align itself in the resulting electromagnetic field. And subsequent applications of charge to neighboring stators would cause the disk to rotate. We have layed out disks for rotation in 11, 7, and sub-degree steps. While smaller steps require smaller actuation voltages, due to larger rotor-to-stator capacitances, more stators, and thus more complex control, may be required.

We should also note that this actuation is due to induced charges on the rotor; furthermore, capacitive area between stators and rotor is limited by the thickness of polysilicon, of which they are comprised. Consequently, large voltages are generally required to generate an acceptable electric field strength. A more thorough analysis of variable capacitance side-drive motors can be found in [1].

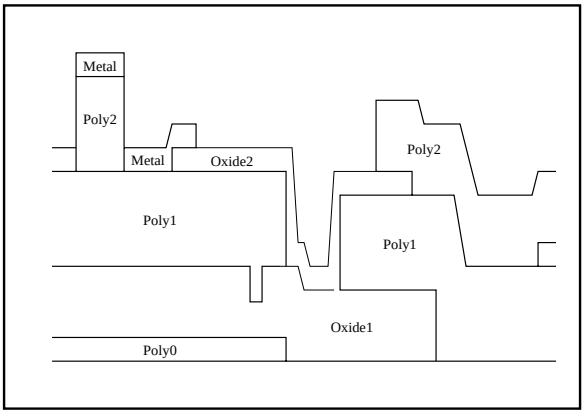

Figure 7: Stator Design

3.3 Re-alignable Mirror Arrays

All of the movable structures discussed in this paper are designed to be actuated electrostatically. The basic model for electrostatic actuation is that of parallel plate capacitors, which follow the equation:

$$F = \sum_{capacitors} \frac{\epsilon V^2 A}{2d^2} \qquad (2)$$

where ϵ is the permittivity, V the applied voltage, A the area of a capacitor plate, and d is distance between the plates.

To actuate our next optical deflector type, re-alignable mirror arrays, we use comb motors [3]. Our implementation of comb motors, discussed in the next section, provide linear actuation, as opposed to rotational, discussed previously. This linear actuation is mechanically converted into a motion that pulls mirrored elements up from the chip surface, at angles up to 20deg (see Figure 8). Three advantages of this deflector design are immediately apparent over the rotation diffraction gratings:

1. the possibility of lower actuation voltages (larger capacitances)
2. continuous alignability (actuation not confined to discrete steps)
3. optical efficiency (function of 0^{th} order rather than 1^{st})

Much more freedom in system configuration is also realized, as the relative positions of emitter, deflector, and detectors is limited neither by minimum feature size of the etching process, nor orientation of the chip surface normal.

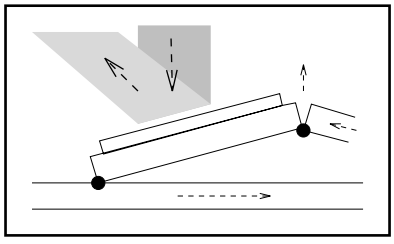

Figure 8: Typical Mirror Element

A tradeoff is seen in the sizing of individual reflective elements. These should be sized to maximize reflective area, relative to that of supporting structures, while keeping voltage, precision of motion, speed, and range of motion in mind. Mechanical hinges in these structures, that allow rotation out of the chip surface,

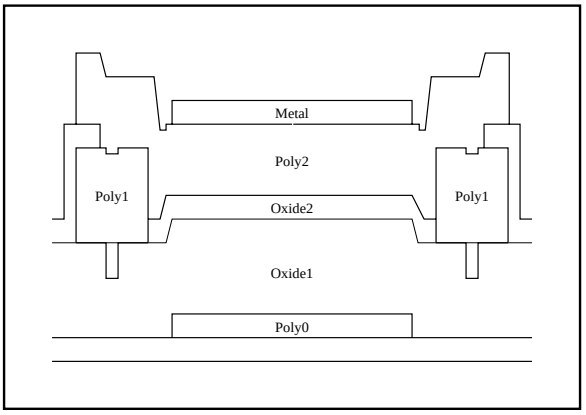

Figure 9: Piston Element Design

are made by one of two methods: either with an approximately square hinge-pin of Poly1 that can freely rotate beneath a bridge of Poly2, or with a thin beam that is allowed to flex, as discussed in Section 4.2.

3.4 Reconfigurable Diffraction Gratings

As with previously mentioned grating designs, the reconfigurable diffraction grating consists of a binary grating structure of reflective metal. In this structure, however, each quantum of the grating is supported by a piston-like structure, that is vertically actuated via electrostatic forces. Thus, an array of these piston-like elements goes together to form, when actuated, a phase-only holographic refractor.

Each piston-like element in this grating array has two stable states: up (natural), and down (activated). Elements are suspended in their 'up' position by beams of Poly2. And their 'down' position is defined by the point at which their support pegs contact the nitride. Instability at intermediate levels of actuation results from material and fabrication non-uniformities, and pull-in capacitance, as discussed in [2].

Our array of elements as shown in the figure were designed for proof of feasibility rather than efficiency; thus reflective metal covers approximately 30% of the array surface, and actuation voltage approximately follows the curve in Figure 10, for elements $67\mu m$ square. We estimate that it would be possible to bring the actuation voltage below 30 volts in the current process.

Despite the required polysilicon deformation, these elements provide a mirror with a very flat surface, in both actuated and non-actuated states. A perimeter of Poly2 ensures that the mirrored membrane remains in tension, raising the Young's moduli almost an order of magnitude over that of the beams.

Sizing of the individual elements and the resulting array should be based on application. It is worth noting, however, that speed and addressability of these reconfigurable diffraction gratings should exceed that of the other devices discussed, due to their small mechanical motion and individually generated actuation forces, respectively.

4 Actuation Methods

4.1 Electrostatic Comb

Electrostatic combs are used to generate sufficient forces for actuation by summing capacitive forces of arrays of polysilicon fingers. The capacitive forces in the y-direction of a comb motor cancel. Deriving Equation 2, to come up with force in the x direction, we get:

$$F = v^2 \left(\frac{\partial C}{\partial x}\right)/2 \tag{3}$$

Using parallel plate approximation, again,

$$\begin{aligned} C &= \sum \frac{\epsilon A}{D} \\ &= N\left[\left(\frac{\epsilon w h}{x_0 - x}\right) + \left(\frac{\epsilon h (l - x_0 + x)}{d}\right)\right] \end{aligned} \tag{4}$$

where N is the number of fingers in the comb, and h is their thickness. But if $x_0 \gg d$, then the rate of change in capacitance with respect to x is a constant, independent of w, l, or x_0:

$$\frac{\partial C}{\partial x} = \frac{N\epsilon h}{d} \tag{5}$$

Since the comb motors we have built use polysilicon springs consisting of two pairs of beams, in the stand-alone case, we have elements that approximately follow:

$$x(L) = \frac{L^3}{6EI}\left[\frac{v^2}{2}\frac{N\epsilon h}{d}\right] \tag{6}$$

4.2 Mechanical Beam Deformation

Several structures rely on the bending moment of polysilicon for motion. Each can be modeled as a beam, fixed at one end, and with a force and moment at the other, as in Figure 12.

The moment is added to the model such that both ends of the beam remain parallel to each other as the beam is deflected. A solution, relating force to displacement, is shown below:

On the model,

Shear:	$V(0)$	$= F$	$V(L)$	$= -F$
Moment:	$M(0)$	$= -FL$	$M(L)$	$= FL$
Angle:	$\theta(0)$	$= 0$	$\theta(L)$	$= 0$
Displacement:	$y(0)$	$= 0$	$y(L)$	$= (?)$

where $y(L)$ describes the displacement at the end of the beam. Using Euler's equation, and its derivatives:

$$\begin{aligned}\frac{V(x)}{EI} &= \frac{d^3y}{dx^3} \qquad (7)\\ &= \frac{1}{EI}\int_0^x W(\eta)d\eta + \frac{F(0)}{EI}\\ &= \begin{cases} +F, & \text{for } x < L/2\ ;\\ -F, & \text{for } x > L/2\ . \end{cases}\end{aligned}$$

$$\begin{aligned}\frac{M(x)}{EI} &= \frac{d^2y}{dx^2} \qquad (8)\\ &= \frac{1}{EI}\int_0^x V(\eta)d\eta + \frac{M(0)}{EI}\\ &= \left[F(L-x) - Fx\right]\frac{1}{EI}\\ &= \frac{F(L-2x)}{EI}\end{aligned}$$

$$\begin{aligned}\theta(x) &= \frac{dy}{dx} \qquad (9)\\ &= \frac{1}{EI}\int_0^x M(\eta)d\eta + \frac{\theta(0)}{EI}\\ &= \frac{+1}{EI}\left[FLx - Fx^2\right], \text{for } x < L/2\ .\end{aligned}$$

$$y(x) = \frac{F}{EI}\left[\frac{L\eta d\eta}{2} - \frac{\eta^3}{3} + 0\right]_0^x \qquad (10)$$

Which reduces, at the end of the beam, to:

$$y(x) = \frac{FL^3}{6EI} \qquad (11)$$

5 Conclusions

The mechanisms presented in this paper for reconfigurable optical interconnect are still under development. Even though many design improvements have yet to be made, we have demonstrated, with these applications and structures presented herein, that the MEMS technology holds potential in the area of high-speed, low-power computing devices. The MEMS device speeds are sufficient for display and scanning devices. And the implementation of reflective-mode optical modulation provides low optical loss and minimal signal latency.

Acknowledgements

The authors wish to thank the following funding and support source: NSF for Dr. Franzon's NSF Young Investigator's Award.

The authors also wish to thank the following individuals for their thoughts and contributions on this research topic: Mouna Nakkar, and Emmanuel Maitre.

References

[1] M. Mehregany, S. F. Bart, L. S. Tavrow, J. H. Lang, S. D. Senturia, and M. F. Schlecht. A study of three microfabricated variable-capacitance motors. *Sensors and Actuators*, A21–A23:173–179, 1990.

[2] Peter M. Osterberg, Raj K. Gupta, John R. Gilbert, and Stephen D. Senturia. Quantitative models for the measurement of residual stress, poisson ratio and young's modulus using electrostatic pull-in of beams and diaphragms. In *Solid-State Sensor and Actuator Workshop*, Hilton Head, SC, June 1994.

[3] William C. Tang, Tu cuong H. Nguyen, and Roger T. Howe. Laterally driven polysilicon resonant microstructures. *Sensors and Actuators*, 20:25–32, 1989.

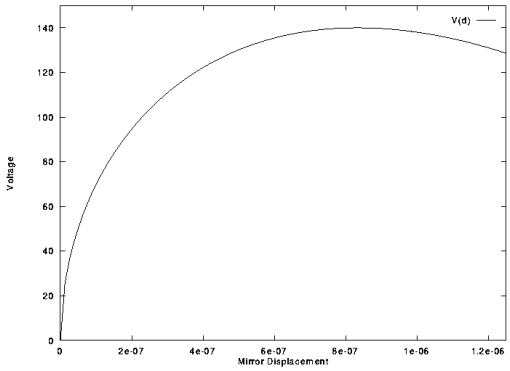

Figure 10: Piston Actuation Curve

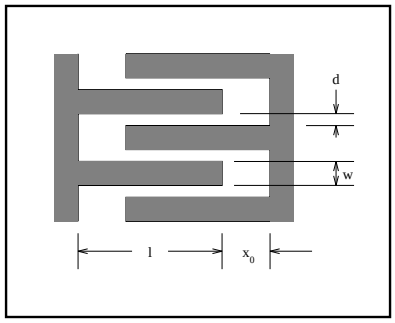

Figure 11: Electrostatic Comb Configuration

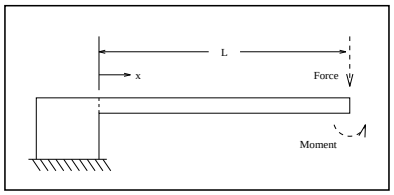

Figure 12: Model of Beam Deformation